The Astrophysical Journal, 646:939–950, 2006 August 1

RED GIANT STARS IN THE LARGE MAGELLANIC CLOUD CLUSTERS[1]

Alessio Mucciarelli
Dipartimento di Astronomia, Università degli Studi di Bologna, Via Ranzani, 1-40127 Bologna, Italy; alessio.mucciarelli@studio.unibo.it

Livia Origlia
INAF—Osservatorio Astronomico di Bologna, Via Ranzani, 1-40127 Bologna, Italy; livia.origlia@bo.astro.it

Francesco R. Ferraro
Dipartimento di Astronomia, Università degli Studi di Bologna, Via Ranzani, 1-40127 Bologna, Italy; francesco.ferraro3@unibo.it

Claudia Maraston
University of Oxford, Denys Wilkinson Building, Keble Road, Oxford, OX1 3RH, UK; maraston@astro.ox.ac.uk

and

Vincenzo Testa
INAF—Osservatorio Astronomico di Roma, Via Frascati, 33-00040 Monteporzio Catone, Italy; testa@mporzio.astro.it
Received 2005 December 18; accepted 2006 April 5

ABSTRACT

We present deep J, H, and K_s photometry and accurate color magnitude diagrams down to $K \approx 18.5$ for a sample of 13 globular clusters in the Large Magellanic Cloud. This data set combined with the previous sample of six clusters published by our group gives the opportunity to study the properties of giant stars in clusters with different ages (ranging from ~80 Myr up to 3.5 Gyr). Quantitative estimates of star population ratios (by number and luminosity) in the asymptotic giant branch (AGB), the red giant branch (RGB), and the He clump have been obtained and compared with theoretical models in the framework of probing the so-called phase transitions. The AGB contribution to the total luminosity starts to be significant at ≈200 Myr and reaches its maximum at 500–600 Myr, when the RGB phase transition is starting. At ≈900 Myr the full development of an extended and well-populated RGB has been completed. The occurrences of both the AGB and RGB phase transitions are sharp events, lasting a few hundred megayears only. These empirical results agree very well with the theoretical predictions of simple stellar population models based on canonical tracks and the fuel-consumption approach.

Subject headings: galaxies: star clusters — infrared: stars — Magellanic Clouds — techniques: photometric

1. INTRODUCTION

The red giant star populations play an important role in the spectral evolution of a simple stellar population (SSP), dominating the bolometric luminosity of a SSP after a few hundred million years. Two special events (the so-called phase transitions [Ph-T's]) due to the sudden appearance of stars with C-O and He degenerate cores mark the spectral evolution of a SSP. The first event corresponds to the appearance of bright asymptotic giant branch (AGB) stars; the second corresponds to the full development of the red giant branch (RGB). Several theoretical models (Renzini & Buzzoni 1986; Bruzual & Charlot 1993; Maraston 1998) investigated the impact of the AGB and RGB stars on the total light of a SSP. The AGB Ph-T is predicted to occur after $\approx 10^8$ yr and the RGB Ph-T after $\approx 6 \times 10^8$ yr. These events must be empirically calibrated by using suitable templates of SSPs, in order to use them for predicting the age of more complex stellar systems such as galaxies. The Large Magellanic Cloud (LMC) globular cluster system represents a gold mine to study the AGB and RGB properties by varying the age and chemical composition of the stellar population. Indeed, these clusters cover a wide range in age (Searle et al. 1980, hereafter SWB; Elson & Fall 1985; Girardi et al. 1995; Brocato et al. 2001), in metallicity (Sagar & Pandey 1989; Olszewski et al. 1991; Hill et al. 2000), and in integrated colors (van den Bergh 1981; Persson et al. 1983), providing the ideal template to investigate the spectral behavior of a SSP.

The AGB and RGB phases are intrinsically difficult to sample with the necessary statistical significance because of their relatively short lifetimes. Several searches investigated the ratio between C and M stars and its correlation with metallicity in the LMC field (Blanco et al. 1980; Cioni & Habing 2003; Cioni et al. 2006), finding more C stars in lower metallicity environments. Frogel et al. (1990, hereafter FMB90) presented a detailed study of C- and M-type AGB stars and their contribution to the cluster total light as a function of SWB classes. FMB90 assumed that the separation between the AGB and RGB is positioned at $M_{\rm bol} = -3.6$ and stars brighter than that value are on the AGB. They found C stars only in the intermediate-age SWB IV–VI clusters. The SWB VII clusters are too old, and their AGB stars have too low mass stellar progenitors for evolving as C stars, while SWB I–III clusters are still too young to have stars evolving along the AGB. In these objects the brightest red stars are M supergiants. For intermediate-age SWB V–VI clusters 40% of the bolometric luminosity is contributed by AGB stars. In particular, C stars, when present, account for 50%–100% of the bolometric luminosity of the AGB. The observational results by FMB90 have been used by Maraston (1998, 2005) to calibrate the energetics and composition of the thermal pulsing phase (TP-AGB) to be inserted in stellar population models. It is therefore very interesting to check those observational results with new, accurate data.

[1] Based on observations collected at the European Southern Observatory, La Silla, Chile, using SOFI at the 3.5 m NTT, within the observing programs 64.N-0038 and 68.D-0287.

TABLE 1
MAIN PARAMETERS OF THE ENTIRE SAMPLE OF OBSERVED LMC CLUSTERS

Cluster	α (J2000.0)	δ (J2000.0)	s	Age (Myr)	[Fe/H]	$E(B-V)$	Reference
NGC 2164	05 58 55.65	−68 31 00.75	23	81	−0.60[a]	0.10	This paper
NGC 2157	05 57 36.74	−69 11 53.58	25	114	−0.60[a]	0.10	This paper
NGC 2136	05 52 58.54	−69 29 32.32	26	135	−0.55[b]	0.10	This paper
NGC 2031	05 33 39.00	−70 59 14.54	27	160	−0.52[b]	0.18	This paper
NGC 1866	05 13 38.88	−65 27 53.30	27	160	−0.50[c]	0.10	This paper
NGC 2134	05 51 57.54	−71 05 51.63	28	190	−1.00[a]	0.10	This paper
NGC 1831	05 06 16.47	−64 55 12.76	31	315	+0.01[d]	0.10	This paper
NGC 2249	06 25 49.50	−68 55 14.25	34	524	−0.12[a]	0.10	F04
NGC 1987	05 27 17.29	−70 43 56.78	35	620	−1.00[a]	0.12	F04
NGC 2209	06 08 34.87	−73 50 06.46	35	620	−1.20[a]	0.07	F04
NGC 2108	05 43 57.30	−69 10 55.93	36	734	−1.20[a]	0.18	F04
NGC 2190	06 01 00.67	−74 43 29.10	36	734	−0.12[d]	0.10	F04
NGC 2231	06 20 43.67	−67 31 13.05	37	869	−0.67[d]	0.08	F04
NGC 1783	04 59 08.42	−65 59 12.75	37	869	−0.45[a]	0.10	This paper
NGC 1651	04 37 33.86	−70 35 09.24	39	1218	−0.37[d]	0.10	This paper
NGC 2162	06 00 30.20	−63 43 15.27	39	1218	−0.23[d]	0.07	This paper
NGC 1806	05 02 11.87	−67 59 10.11	40	1442	−0.23[d]	0.12	This paper
NGC 2173	05 57 59.28	−72 58 42.83	42	2021	−0.24[d]	0.07	This paper
NGC 1978	05 28 45.34	−66 14 09.12	45	3353	−0.96[c]	0.10	This paper

NOTES.— Units of right ascension are hours, minutes, and seconds, and units of declination are degrees, arcminutes, and arcseconds. The s-parameter is from Elson & Fall (1985) and Girardi et al. (1995). Reddening is from Persson et al. (1983).
[a] Sagar & Pandey (1989).
[b] Dirsch et al. (2000).
[c] Hill et al. (2000).
[d] Olszewski et al. (1991).

The first observational evidence of the RGB Ph-T in stellar clusters was presented by Ferraro et al. (1995, hereafter F95), who analyzed the red giant contents of 12 intermediate-age LMC clusters. This survey was performed with the first generation of IR imagers and sampled only the brightest portion ($K < 14.3$) of the RGB. Despite its limited luminosity sampling, this pioneering work demonstrated that near-IR observations are indeed crucial in order to study the photometric properties of AGB and RGB sequences, providing the highest sensitivity to the physical parameters of cool stars.

Recently, the superior performances of the 1024×1024 IR array detector of Son of Isaac (SOFI) at the European Southern Observatory (ESO) New Technology Telescope (NTT) allowed measurement the entire extension of the RGB for a complete sample of LMC clusters spanning a wide range of ages. Ferraro et al. (2004, hereafter F04) presented deep J, H, and K_s photometry and accurate color magnitude diagrams (CMDs) down to $K \approx 18.5$, i.e., $\approx$1.5 mag below the red He clump, for six intermediate-age clusters (namely, NGC 1987, NGC 2108, NGC 2190, NGC 2209, NGC 2231, and NGC 2249). A quantitative estimate of the population ratios (by number and luminosity) between RGB and He-clump stars for each target cluster and comparison with theoretical predictions suggest that the full development of the RGB should occur at $t \approx 700$ Myr and be a relatively fast event ($\delta t \approx 300$ Myr).

The present paper shows the results for 13 additional LMC clusters, extending the discussion about the RGB Ph-T presented in F04 and studying the contribution to the total luminosity of the AGB. The paper is organized as follows: § 2 describes the observations and photometric analysis and § 3 the near-IR CMDs. Section 4 presents the basic assumptions on reddening and the adopted age calibration. Section 5 discusses the procedure adopted to derive complete and accurate star counts and the luminosity contribution. Sections 6 and 7 discuss the phase transitions, while in § 8 we draw our conclusions.

2. OBSERVATIONS AND PHOTOMETRIC ANALYSIS

J, H, and K_s images of 13 globular clusters in the LMC (see Table 1) have been obtained at ESO, La Silla, on 2001 December 28–30 with the near-IR imager/spectrometer SOFI (Moorwood et al. 1998) mounted at the ESO 3.5 m NTT. SOFI is equipped with a 1024×1024 Rockwell IR-array detector. All the observations presented here have been performed with a scale of $0''.292$ pixel^{-1}, providing a $\approx 5' \times 5'$ field of view for each frame. The observations were obtained in good seeing conditions ($0''.7$–$0''.8$ on average). Total integration times of 2 minutes in J, 4 minutes in H, and 8 minutes in K_s split into sets of shorter exposures have been secured, allowing us to obtain accurate (signal-to-noise ratio [S/N] of $\geq$30) photometry down to $J \approx 19$ and H and $K_s \approx 18.5$.

Clusters have been selected according to the s-parameter, defined by Elson & Fall (1985) as a curvilinear coordinate running along the mean locus defined by the $(U-B)$ and $(B-V)$ integrated colors of the LMC clusters and directly linked to the cluster age. The six clusters presented by F04 have s-parameters ranging between 34 and 37. The data presented here include seven additional clusters with $s = 23$–31 and six with $s = 37$–45. Table 1 lists the basic properties of the clusters discussed in the paper: s-values (Elson & Fall 1988), $E(B-V)$ (Persson et al. 1983), and metallicity (Sagar & Pandey 1989; Olszewski et al. 1991; Hill et al. 2000; Dirsch et al. 2000). Indicative [Fe/H] values vary by a factor of $\approx$10, between -1.2 and solar with an average value of $\approx -0.6 \pm 0.1$, but precise abundance determinations via high-resolution spectroscopy are still lacking for the majority of the LMC clusters.

A control field a few arcminutes away from each cluster center has also been observed using the same instrumental configuration, in order to construct median-averaged sky frames and for

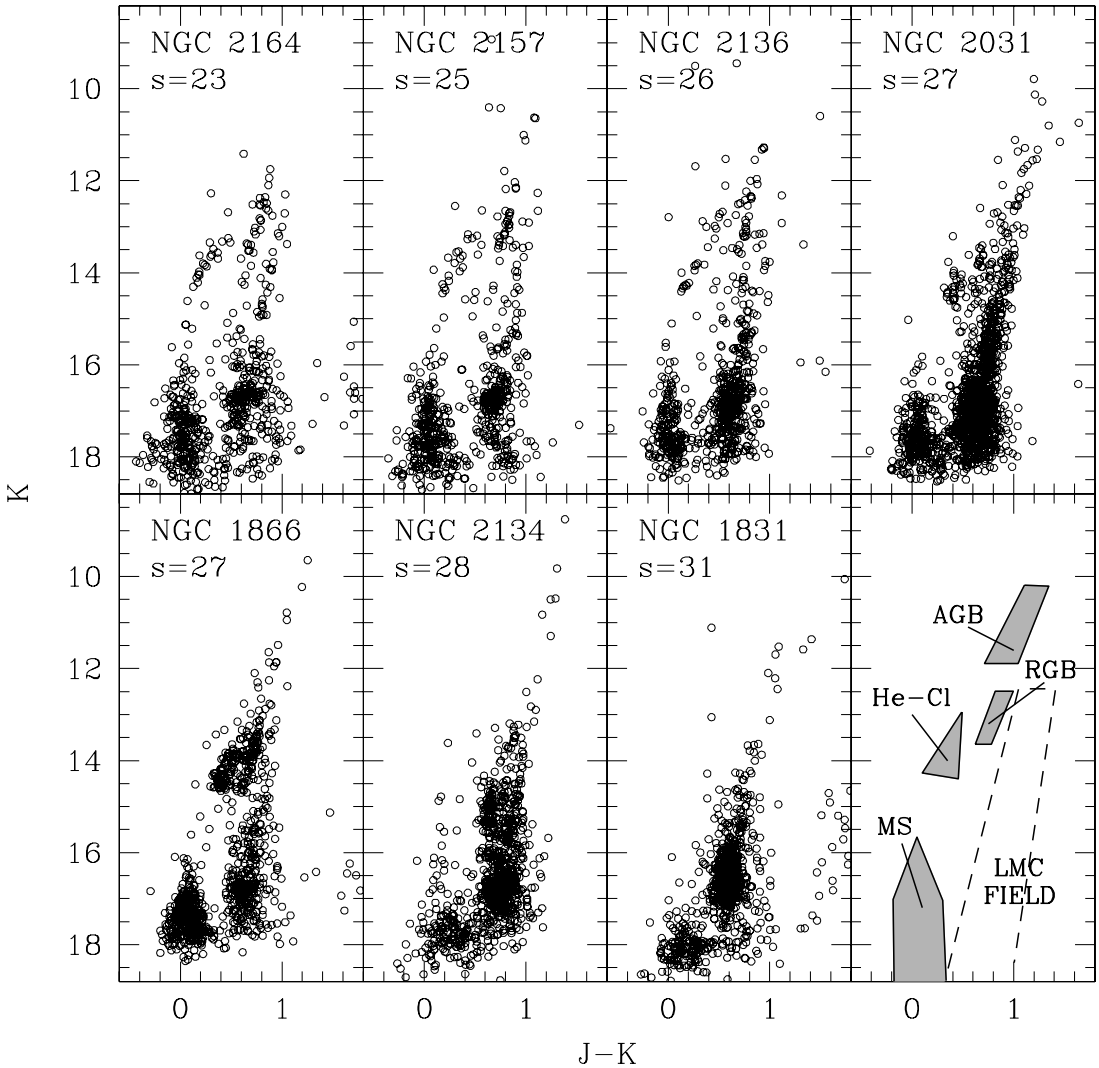

FIG. 1.—Observed ($K, J-K$) CMDs of the seven observed LMC clusters with $s = 23$–31. In the bottom right panel a sketch of the CMD loci dominated by the cluster (*gray regions*) and the LMC field (*dashed box*) populations are also shown for sake of clarity.

decontamination purposes. A large sample of high-S/N flat fields in each filter have been acquired by using a halogen lamp, alternatively switched on and off. The final cluster and control field frames have been sky-subtracted and flat-field corrected. For each cluster, the data set includes three J, H, and K_s images centered on the cluster and three corresponding frames of an adjacent field.

The photometric analysis was performed by using DAOPHOT II (Stetson 1987). For each observed field all the images in the J, H, and K_s filters were carefully aligned and trimmed in order to have three output images, one per filter, slightly smaller than the original ones but perfectly registered. Then a DAOPHOT II point-spread function (PSF) fitting run was applied to each image. The output catalog with the instrumental magnitudes has been checked for any spurious detection or missing objects (typically 3–4 stars at most), which have been included in the catalog by hand.

Each catalog typically contains 1000–1200 stars, with the exception of three poorly populated clusters counting less than 700 stars (NGC 1651, NGC 2162, and NGC 2173) and two rich clusters with more than 1900 stars (NGC 1783 and NGC 1978). The instrumental magnitudes have been transformed into the Two Micron All Sky Survey (2MASS) photometric system, by using the large number of stars (typically a few hundred) in common. The overall dispersion of these transformations is $\sigma \leq 0.01$ mag in all three filters. For sake of homogeneity, the output catalogs of F04 (calibrated on the Persson et al. [1998] photometric system) have been also transformed into the 2MASS one, although the difference between the two calibrations turns out to be negligible ($\approx$0.01 mag).

The calibrated photometric catalogs in each filter were finally matched and merged together in a global catalog, using the CATAXCORR and CATACOMB software developed at the Bologna Observatory for an optimized cross-correlation.

3. COLOR-MAGNITUDE DIAGRAMS

Figures 1, 2, 3, and 4 show the CMDs for the observed clusters and adjacent fields in the (K, ($J-K$))-plane. We have divided the clusters into two groups, according to their s-parameter and different CMD morphology. The first group (see Fig. 1) includes clusters with $s = 23$–31; the second group (see Fig. 3) includes those with $s = 37$–45. Figures 2 and 4 show the CMDs of the corresponding adjacent fields.[2]

[2] The extreme field contamination for NGC 2031, located in the LMC bar, is evident.

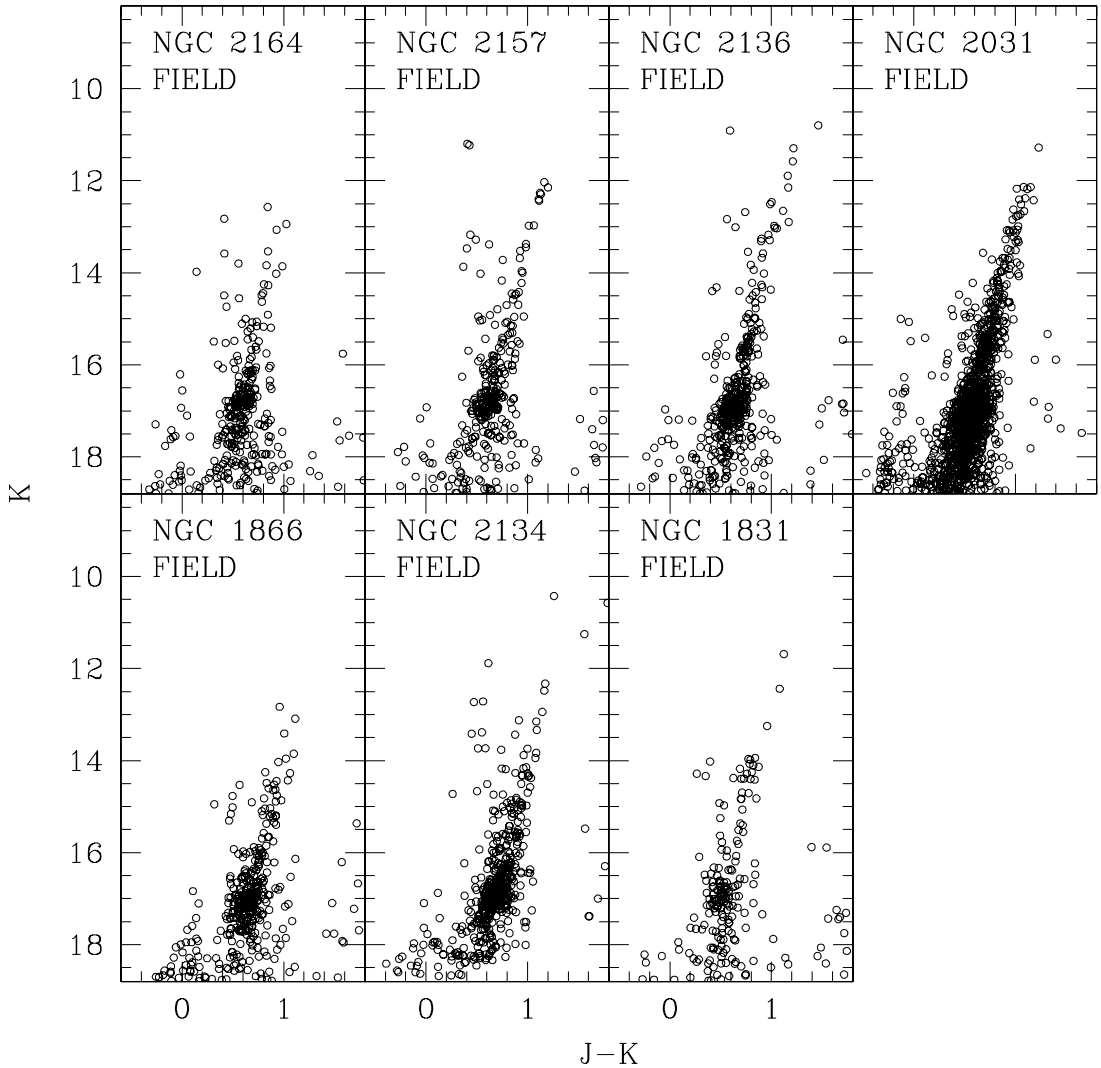

FIG. 2.—Same as Fig. 1, but of the fields adjacent to the seven observed LMC clusters with $s = 23$–31.

The CMDs of the first group of clusters (with $s < 31$) appear quite complex; hence, particular care has been devoted to separate the cluster population from the LMC field. In order to help the reader identify the two populations we have plotted in the last panel of Figure 1 a sketch showing the mean location of cluster (*gray regions*) and field (*dashed box*) population in the CMD. The main properties of the CMDs shown in Figure 1 can be summarized as follows:

1. Magnitudes as faint as $K \approx 18.5$ have been measured.
2. The brightest objects at $K < 13$ are likely AGB stars.
3. A blue sequence is clearly visible at $-0.3 < (J - K) < 0.3$ and $K > 15.5$, corresponding to the brightest end of the cluster main sequence (MS).
4. Helium-clump cluster stars define a sequence at $K = 13$–14 and $(J - K) \sim 0.2$ in the youngest objects (namely, NGC 2164, NGC 2157, and NGC 2136). In older clusters (namely, NGC 2031, NGC 1866, NGC 2134, and NGC 1831), they define a clump at progressively lower magnitudes ($K = 14$–15) and redder colors $[0.4 < (J - K) < 0.6]$.
5. The direct comparison of each panel in Figures 1 and 2 clearly shows the significant contribution of the LMC field stars. As schematically shown in the last panel of Figure 1, most of the stars in the region $0.4 < (J - K) < 1$ and $K > 12$ are indeed LMC field stars, with a well-defined RGB at $12 < K < 16$ and the He clump at $K \approx 17$.

The observed CMDs for the second group of clusters show the following characteristics:

1. They have magnitude limits down to $K \approx 18.5$, i.e., about 1.5 mag below the He clump, which is clearly visible as a clump of stars at $K \approx 17$.
2. The have a well-populated and extended RGB.
3. The brightest objects at $K < 12$ are likely AGB stars.
4. Unlike the first group of clusters, in these objects cluster and field populations do overlap.

4. BASIC ASSUMPTIONS

4.1. *Reddening*

Correction for extinction is computed according to the $E(B - V)$-values reported in Table 1 and the Rieke & Lebofsky (1985) interstellar extinction law. The infrared dust maps by Schlegel et al. (1998) in the direction of the observed clusters provide very similar (on average within ± 0.03 dex) $E(B - V)$ corrections, with the exception of NGC 2031, for which the discrepancy is about 0.1 dex. However, the overall impact of such a

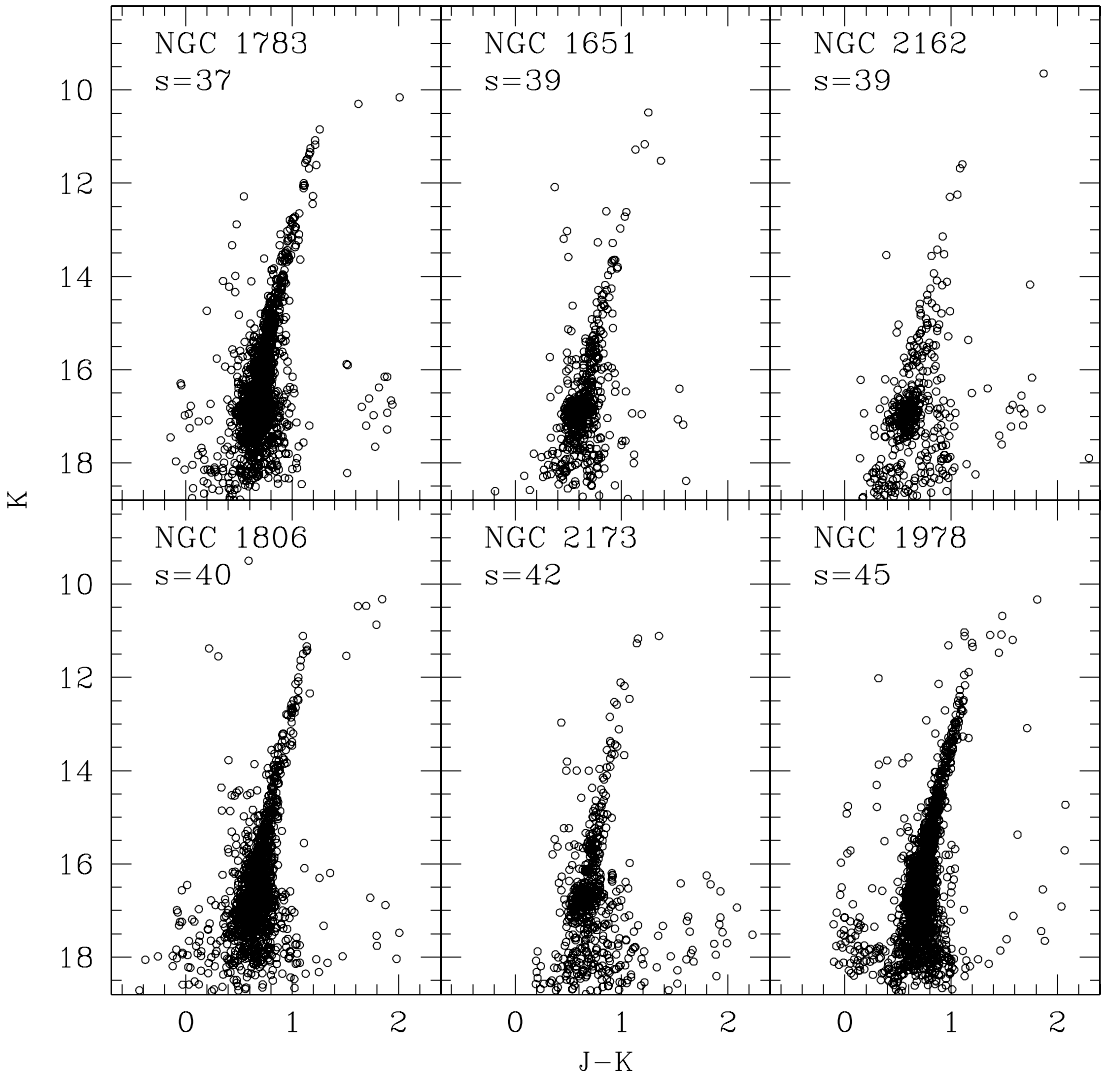

FIG. 3.—Same as Fig. 1, but of the six observed LMC clusters with $s = 39–45$.

discrepancy on the infrared magnitudes is always small (well within 0.1 dex); hence, reddening correction is not a critical issue in this context.

Absolute and bolometric magnitudes have been obtained by adopting a distance modulus $(m - M)_0 = 18.5$ (van den Bergh 1998; Alves 2004) and suitable bolometric corrections by using the $(J - K)_0$ color and the empirical calibrations by Montegriffo et al. (1998). In computing luminosities, we adopted $M_\odot^{\rm bol} = 4.74$ and $M_\odot^K = 3.41$ for the Sun. In the following all the derived luminosities are expressed in units of $10^4\ L_\odot$.

4.2. *Age Calibration*

A suitable calibration of the LMC cluster age is still a major concern, since homogeneous determinations based on the MS turn-off, for a significant number of clusters, are not available yet. Following F04, here we use the *s*-parameter (see § 2). Being a pure empirical quantity, it needs to be calibrated with age. As discussed in F04, the most used calibrations by Elson & Fall (1988) based on canonical models and by Girardi et al. (1995) based on overshooting models provide, somewhat surprisingly, very similar ages (within 10%–15%). Although a new calibration of the *s*-parameter as a function of age (see F04) is urged, in the following, as done in F04, we adopted the most recent one by Girardi et al. (1995) and based on the models with overshooting by Bertelli et al. (1994):

$$\log t = 6.227 + 0.0733s.$$

We assume a conservative error of $\delta s = \pm 1$, which translates into a ≈20% age uncertainty.

Table 1 lists the *s*-values for the entire sample of 19 clusters (13 presented here and six discussed in F04) and their ages derived from the quoted calibration. As can be seen the entire sample covers a large range of ages from 80 Myr to 3.5 Gyr.

5. STAR COUNTS AND INTEGRATED LUMINOSITIES

A quantitative analysis of the AGB and RGB populations (by number and luminosity) is crucial to empirically calibrate the relative lifetimes and to quantitatively evaluate the impact of each evolutionary stage on the total luminosity of a SSP. In order to obtain reliable stellar counts and luminosities in each branch, we proceeded as follows: (1) stars in each evolutionary stage have been identified on the basis of suitable selection boxes as defined

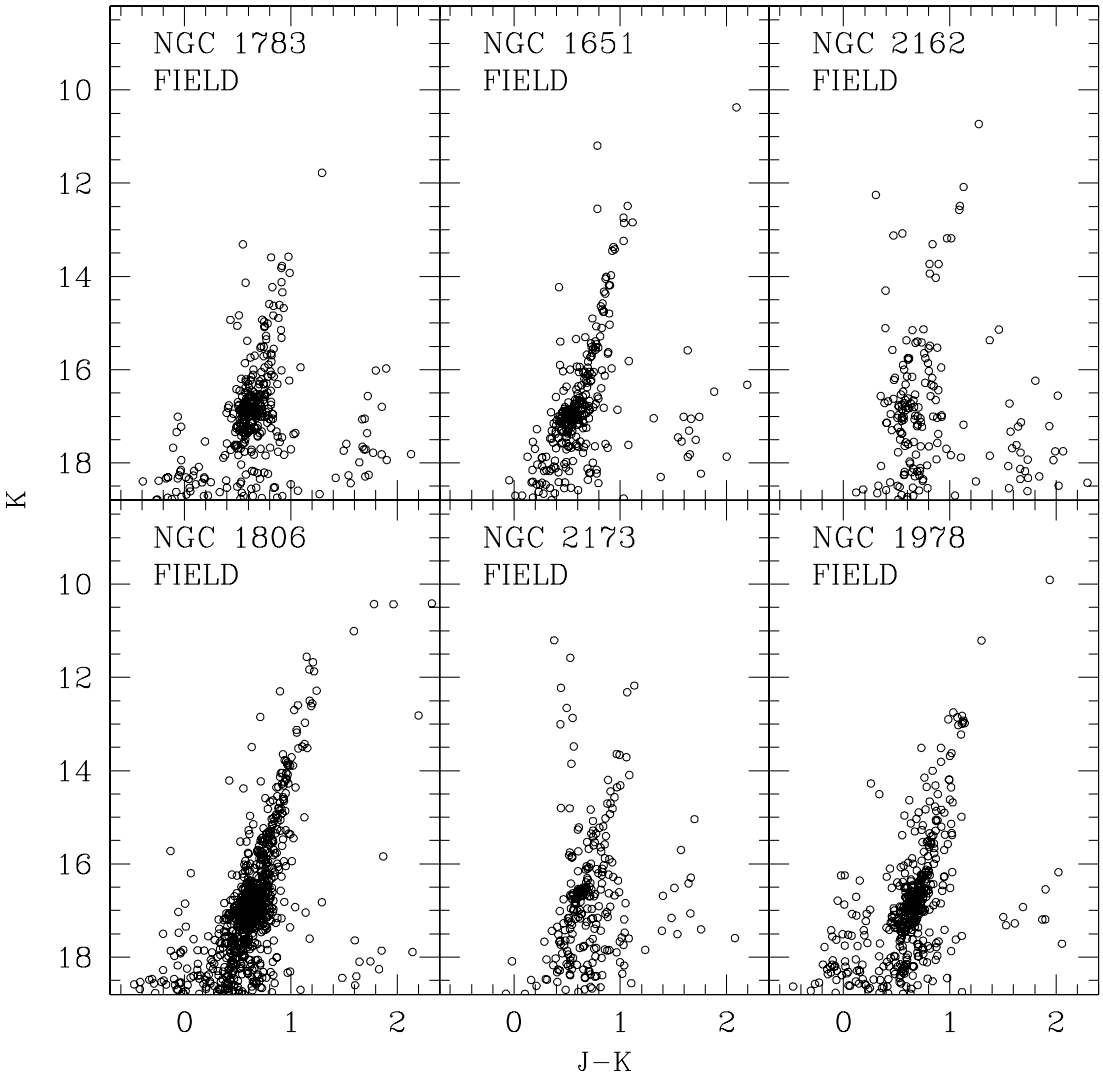

FIG. 4.—Same as Fig. 1, but of the fields adjacent to the six observed LMC clusters with $s = 39–45$.

in the CMDs (as shown in Figs. 6 and 9); (2) each sample of stars has been corrected for incompleteness, following the standard "artificial star" technique (see below); and (3) the contamination from foreground/background stars in each population has been evaluated and statistically subtracted from the observed samples.

While the definition of the selection boxes (step 1) for the AGB and RGB populations are described in §§ 6 and 7, respectively, in the following we briefly discuss the procedure adopted to perform steps 2 and 3.

5.1. *Completeness and Field Decontamination*

The degree of completeness can be quantified by using the widely used artificial star technique (see the discussion in Mateo 1988). For each cluster we have derived the RGB fiducial line, and then a population of artificial stars, having magnitudes, colors, and luminosity functions resembling the observed distributions, was generated and added to the original images. Since crowding effects are more severe in the central regions, the frame area sampling the cluster has been divided in three concentric regions (see Fig. 5, *left*, *regions* A, B, *and* C), and the completeness has been estimated independently in each of them. The maximum spatial extension of each cluster has been estimated from the cluster radial density profile. A total of ≈200,000 artificial stars have been simulated in each cluster in about 1000 simulation runs. Indeed, in order not to alter the crowding conditions, only 100–200 stars have been simulated in each run. The fraction of recovered objects in each magnitude interval was estimated as $\Lambda = N_{\rm rec}/N_{\rm sim}$, and a suitable completeness curve was obtained in each of the regions (see Fig. 5, *right*).

Finally, star counts in each radial region have been corrected for incompleteness, by dividing each observed distribution by the corresponding Λ-factors.[3] The total number of stars has been finally obtained by summing the completeness-corrected number of stars of regions A, B, and C.

As already discussed in previous papers, the artificial star technique provides only a first-order correction. In fact, the observed distribution is, in principle, distorted because of two main phenomena: the loss of faint stars due to incompleteness and an excess of bright stars due to possible blending effects of two or

[3] Note that the number of stars lost for incompleteness ($n_{\rm comp}$) in each bin of magnitude is

$$n_{\rm comp} = n_{\rm obs}(1/\Lambda - 1),$$

where $n_{\rm obs}$ is the number of stars observed in that bin.

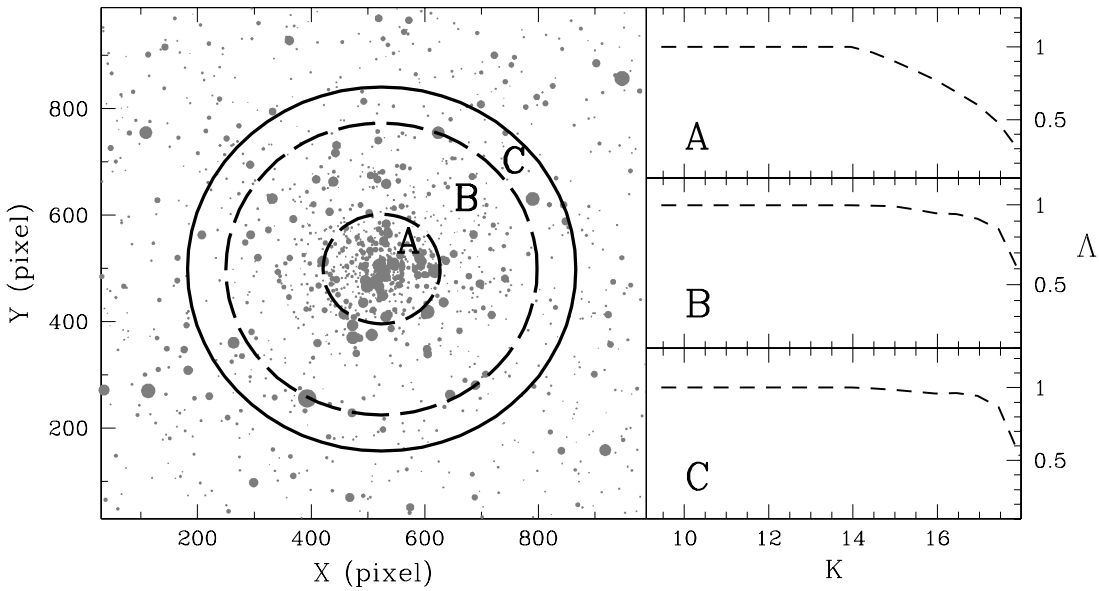

FIG. 5.—Example of cluster radial mapping. *Left:* Cluster frame divided into three concentric annuli, to account for different crowding conditions. *Right:* Completeness curve for each radial subregion, as labeled in the left panel.

more faint stars into a brighter one. Only the first effect is taken into account by the artificial star simulation. Blending from faint MS stars is a more complicated effect to simulate; however, in the near-IR it is negligible (see also the discussion in Testa et al. 1999).

Another important effect that needs to be investigated is the degree of contamination of the selected samples by the foreground/background stars. In this paper we have applied a statistical decontamination technique, using a control field adjacent to the clusters. The total number of stars observed in each evolutionary sequence (AGB, RGB, and He clump) has been counted according to the selection boxes both in the cluster (see Figs. 1 and 3) and in the field (see Figs. 2 and 4) CMDs and corrected for incompleteness (see above). The star counts in the field population have been scaled to take into account the different surveyed area, and their contribution has been subtracted from the cluster population.

In summary, for each radial region, each selection box corresponding to each evolutionary stage has been divided in bins of magnitude (typically 0.2 mag wide). Then the "corrected" number of stars in each bin has been computed as follows:

$$n_{\rm corr} = n_{\rm obs} + n_{\rm comp} - n_f,$$

where $n_{\rm obs}$ is the number of stars observed in that bin, $n_{\rm comp}$ is the number of stars lost for incompleteness, and n_f is the expected number of field stars.

Analogously, the total luminosity of each evolutionary stage can be computed according to the following relation:

$$L_{\rm corr} = \sum_{i=1}^{n} L_i^{\rm obs} + n_{\rm comp} L_{\rm eq} - n_f L_{\rm eq},$$

where the term $\sum_{i=1}^{n} L_i^{\rm obs}$ is the total luminosity of the stars observed in a given bin, $n_{\rm comp}$ is the number of stars lost for incompleteness, n_f is the expected number of field stars, and $L_{\rm eq}$ is the equivalent luminosity of that bin, which is the luminosity of a star with magnitude equal to the mean value of the bin.

Finally, the star counts and total luminosity of each evolutionary stage have been obtained by summing the contribution of all the bins in each selection box.

5.2. *Integrated Magnitudes*

In order to properly perform cluster-to-cluster comparisons, one needs to take into account the size of the total cluster population. Hence, both star counts and luminosities need to be normalized to a reference population or to the cluster integrated luminosity. In previous papers we followed both of the approaches (in F95 and F04 the RGB populations were normalized to the cluster integrated luminosity taken from the literature and to the He-clump population, respectively).

The large field of view of SOFI offers the opportunity to independently determine the near-infrared integrated magnitudes for the program clusters. In doing this, we adopted a simple approach, by performing aperture photometry over the entire cluster extension (typically 90″). In order to correct for the field contamination, an equivalent aperture photometry has also been performed on each control field, and the resulting luminosity has been subtracted from the cluster value.

The cluster center has been computed by applying a standard technique (see, e.g., Calzetti et al. 1993) that uses the knowledge of the positions of individual stars in the innermost region of the cluster, allowing a high-precision determination of the center of gravity. Hence, by applying the procedure described in Montegriffo et al. (1995) we computed $C_{\rm grav}$ by simply averaging the α- and δ-coordinates of stars lying within a fixed radius from a first-guess center estimated by eye. The barycenter of the stars is then derived iteratively (see also Ferraro et al. 2003). The center of gravity ($C_{\rm grav}$) of the program clusters are listed in Table 1. Our new estimates turn out to be reasonably consistent (within ~10″) with available determinations (as those in the SIMBAD astronomical database by the CDS, Strasbourg). The typical 1 σ uncertainty of our estimates is ~5 pixels corresponding to 1″.5 in both $\alpha_{\rm J2000}$ and $\delta_{\rm J2000}$. The positions of the centers of two clusters, namely, NGC 2136 and NGC 2173,

TABLE 2
Integrated K Magnitude, Colors, and Luminosities of the Target Clusters

Cluster	s	K	$J-K$	$H-K$	$L^K_{\rm tot}$ ($10^4\ L_\odot$)	$L^{\rm bol}_{\rm tot}$ ($10^4\ L_\odot$)
NGC 2164	23	8.575	0.606	0.122	19.76	12.82
NGC 2157	25	8.286	0.658	0.195	25.79	15.18
NGC 2136	26	7.968	0.674	0.125	34.57	19.78
NGC 2031	27	8.219	0.936	0.323	28.14	11.36
NGC 1866	27	7.282	0.743	0.155	65.02	33.13
NGC 2134	28	9.161	0.742	0.187	11.52	5.88
NGC 1831	31	8.313	0.802	0.231	25.16	11.67
NGC 2249	34	9.983	0.934	0.342	5.40	2.06
NGC 1987	35	8.811	0.988	0.316	16.00	5.75
NGC 2209	35	8.955	1.224	0.345	13.79	3.54
NGC 2108	36	8.807	1.148	0.403	16.38	4.96
NGC 2190	36	9.269	1.193	0.321	10.43	2.83
NGC 2231	37	9.329	1.096	0.328	9.81	2.97
NGC 1783	37	7.091	1.035	0.282	77.53	25.77
NGC 1651	39	8.895	0.973	0.301	14.72	5.32
NGC 2162	39	9.071	1.253	0.372	12.40	3.07
NGC 1806	40	7.076	1.055	0.271	79.11	25.97
NGC 2173	42	9.05	1.033	0.297	12.33	4.02
NGC 1978	45	7.185	0.894	0.288	71.10	28.69

Note.—Integrated magnitudes are decontaminated for the field contribution.

appear to be significantly (up to 2′) different from the SIMBAD coordinates.

The case of NGC 2136 deserves additional comment. Indeed, a small *twin* cluster, namely, NGC 2137, is present at an angular distance of 1.′34 (Hilker et al. 1995). Since its integrated luminosity, although significantly fainter, is contaminating the aperture photometry of NGC 2136, it has been properly subtracted.

Integrated K magnitude, colors, and derived luminosities in the K band and in bolometric for the entire sample of 19 clusters are listed in Table 2.

5.3. *Error Budget*

Formal errors are directly estimated from the photometric samples, by assuming that star counts follow Poisson statistics. The error bars for the various population ratios (by number and/or by luminosity) have been computed according to the following formula:

$$\sigma_R = \frac{\sqrt{R^2\sigma_D^2 + \sigma_N^2}}{D},$$

with $R = N/D$, where N is the numerator and D the denominator of the ratio.

In the computation of the population ratios, different error sources are at work, depending on the observable.

Total cluster luminosity.—The main source of uncertainty in this case is the positioning of the cluster center. We estimate that an off-centering of 5 pixels corresponds to a 5% variation in luminosity. An additional uncertainty of ≈10% has been considered in the computation of bolometric luminosities, in order to take into account the uncertainty in the bolometric corrections.

AGB luminosity.—A conservative uncertainty of 0.2 mag in setting the faint end of the AGB luminosity distribution implies a ≈5% variation in the total AGB luminosity. However, for this observable the major source of uncertainty is the random error associated to the number of detected AGB stars [in the Poisson regime $\sigma \propto (N_{\rm AGB})^{1/2}$], which can suffer large fluctuations due to small-number statistics. On average, the overall σ_R associated with the $L^K_{\rm AGB}/L^K_{\rm tot}$ ratio turns out to be 30%.

Number and luminosity of C stars.—As in the case of AGB stars, these observables and their associated errors suffer large fluctuations due to small-number statistics. On average, the overall σ_R associated with the $L^K_{\rm C\ star}/L^K_{\rm tot}$ ratio turns out to be ≈50%.

RGB luminosity.—In the older clusters (see Fig. 3) the RGB is well populated; hence, the estimated luminosity is much less affected by statistical fluctuations or by the selection box definition. On average, we estimate $\sigma_R \approx 20\%$ for the RGB population ratios.

6. THE AGB AND C-RICH STAR CONTRIBUTION TO THE CLUSTER LIGHT

Theoretical models (Renzini & Buzzoni 1986; Maraston 1998, 2005) predict that the most important contributors to the integrated cluster light between 10^8 and 10^9 yr are AGB stars. The AGB population includes both O-rich (M type) and C-rich stars. During the thermal pulsing phase (TP-AGB) an AGB becomes C-rich if it undergoes the third dredge-up mixing process (see, e.g., Iben & Renzini 1983). The presence of C stars in stellar clusters depends on their age and metallicity (Renzini & Voli 1981).

In intermediate-age clusters the bulk of the AGB population is more luminous than the RGB tip, and a minor overlap does exist between the faintest end of the AGB and the brightest portion of the RGB. Here we use our data set in order to investigate the contribution to the cluster luminosity of the brightest portion of the AGB populations as a function of the cluster age. In order to consider the entire database, which spans a large range of ages (from 80 Myr to 3.5 Gyr; see Table 1), in the following we consider only AGB stars brighter than $K \approx 12.3$, which represents the RGB tip level for the oldest clusters in our sample (see F04).

The left panel of Figure 6 shows the brightest portion of the K_0, $(J-K)_0$ cumulative CMD, where all the stars detected in the 19 surveyed clusters are plotted. The selection box adopted to sample the bright AGB population is overplotted in the diagram. The right panel of Figure 6 shows the cumulative $(J-H)_0$, $(H-K)_0$ color-color diagram for the selected AGB stars. This

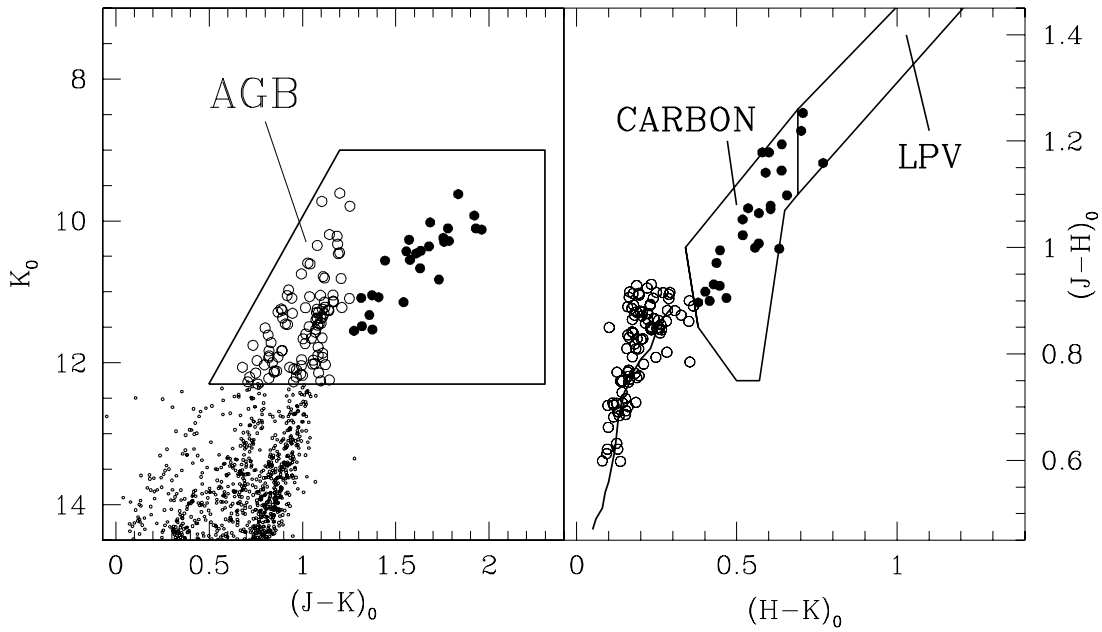

FIG. 6.—*Left:* Cumulative, dereddened K_0, $(J-K)_0$ CMD for the entire cluster sample. The selection box adopted to isolate the AGB population (*large circles*) is shown. *Right:* Dereddened color-color $(J-H)_0$, $(H-K)_0$ diagram of the AGB stars. In both panels open circles are O-rich AGB stars and filled circles are C stars. The boxes to distinguish C stars and long-period variables (LPVs) are from Bessell & Brett. (1988; see also F95). The mean locus for K giant stars (*solid line*) is from Frogel et al. (1978).

diagram is especially suitable to isolate C stars, since they are significantly redder than O-rich stars (see also Cioni et al. 2006). As shown in Figure 6 a population of 26 candidate C stars (*filled circles*) has been identified on the basis of their extremely red colors in the 19 surveyed clusters.

Note also that the artificial star experiments demonstrated that stars lying in the brightest portion of the RGB can be safely recovered (with an overall photometric uncertainty of ~0.03 mag) even in the innermost region of the clusters, excluding the possibility that blending of RGB stars could produce spurious bright objects lying within the AGB selection box.

We used both the cumulative color-magnitude and color-color diagrams in Figure 6 to make a census (both by number and by luminosity) of the AGB stars brighter than the RGB tip, as well as of C stars in each cluster. Although the number and the luminosity of AGB stars are subject to large fluctuations due to small-number statistics, we still performed a statistical decontamination, following the procedure described in § 5.1.

The number of AGB stars counted in each cluster and the number adopted after the field decontamination are listed in Table 3. Once an accurate census of the AGB population (by number and luminosity) is available for all the sampled clusters, a number of

TABLE 3
STAR COUNTS AND LUMINOSITIES FOR AGB AND C STARS

Cluster	s	$N_{\rm AGB}^{\rm obs}$	$N_{\rm AGB}^{\rm field}$	$N_{\rm AGB}^{\rm dec}$	$L_{\rm AGB}^K/L_{\rm tot}^K$	$N_{\rm C\ star}$	$N_{\rm C\ star}/L_{\rm tot}^{\rm bol}$	$N_{\rm C\ star}/L_{\rm tot}^K$	$L_{\rm C\ star}^K/L_{\rm tot}^K$
NGC 2164	23	2	0	2	0.10	0	0	0	0
NGC 2157	25	9	1	8	0.52	0	0	0	0
NGC 2136	26	9	1	8	0.31	1	0.05	0.03	0.09
NGC 2031	27	7	1	6	0.64	0	0	0	0
NGC 1866	27	12	0	12	0.36	0	0	0	0
NGC 2134	28	2	1	1	0.71	0	0	0	0
NGC 1831	31	7	1	6	0.45	3	0.26	0.12	0.31
NGC 2249	34	1	0	1	0.32	0	0	0	0
NGC 1987	35	9	4	5	0.90	3	0.52	0.19	0.61
NGC 2209	35	4	0	4	0.72	2	0.56	0.14	0.58
NGC 2108	36	5	1	4	0.87	1	0.20	0.06	0.34
NGC 2190	36	2	0	2	0.74	2	0.71	0.19	0.72
NGC 2231	37	1	0	1	0.32	1	0.34	0.10	0.32
NGC 1783	37	16	1	15	0.36	2	0.08	0.03	0.11
NGC 1651	39	4	0	4	0.51	1	0.19	0.07	0.09
NGC 2162	39	4	1	3	0.73	1	0.32	0.08	0.59
NGC 1806	40	13	4	9	0.22	4	0.15	0.05	0.17
NGC 2173	42	5	1	4	0.53	1	0.25	0.08	0.15
NGC 1978	45	13	1	12	0.25	4	0.14	0.06	0.13

NOTES.—Star counts are corrected for incompleteness. K-band and bolometric luminosities are in units of $10^4\ L_\odot$.

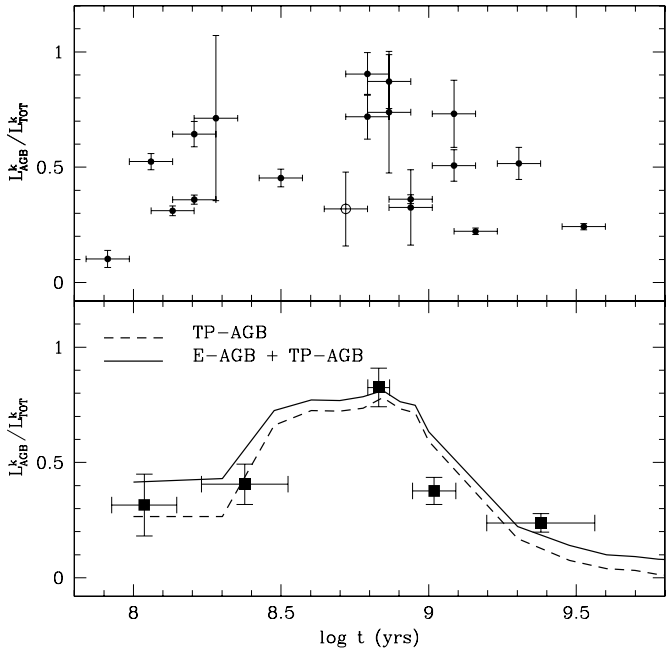

FIG. 7.—*Top:* Observed AGB contribution to the total cluster *K*-band luminosity as a function of age. The open circle marks the intrinsically poor populated cluster NGC 2249. *Bottom:* Weighted mean and standard deviation of the same ratio with the clusters grouped into five age bins, according to their *s*-parameter, namely, $s = 23$–26, 27–31, 35–36, 37–39, and 40–45 (the cluster NGC 2249 has been excluded). Theoretical predictions for the temporal evolution of the entire AGB (E-AGB and TP-AGB, *solid line*) and for the dominant TP-AGB (*dashed line*) are overplotted. Both models are computed at $[Z/\mathrm{H}] = -0.33$.

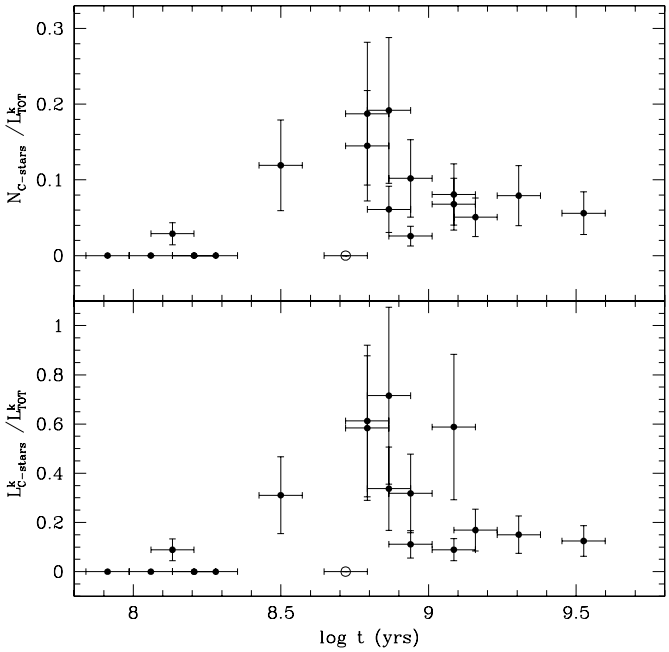

FIG. 8.—*Top:* Number of C stars normalized to the *K*-band luminosity of the cluster as a function of age. *Bottom:* *K*-band luminosity of the C stars normalized to the total cluster luminosity as a function of age. The open circles mark the intrinsically poor populated cluster NGC 2249.

suitable diagnostics tools can be used in order to study the AGB properties as a function of the age.

The top panel of Figure 7 shows the ratio between the AGB and the cluster integrated *K*-band luminosity, as a function of the cluster age. It is remarkable that the AGB luminosity increases rapidly (up to a factor of 2) at ≈200 Myr, reaching its maximum contribution in the 300–700 Myr range, followed by a rapid decrease. Note that in two clusters (namely, NGC 2108 and NGC 1987 at $s = 35$–36 corresponding to $t \sim 600$–700 Myr) the brightest portion of the AGB population accounts for ≈90% of the total cluster luminosity. These results are in good agreement with F95, who found that the maximum contribution of the AGB to the cluster light occurs at $s = 35$, corresponding to an age of ≈600 Myr.

The bottom panel of Figure 7 shows the same ratio as in the top panel but with the clusters grouped into five age bins according to their *s*-parameter, namely, $s = 23$–26, 27–31, 35–36, 37–39, and 40–45. For each bin we computed the weighted mean and the corresponding standard deviation. Theoretical predictions from Maraston (1998, 2005) for $[Z/\mathrm{H}] = -0.33$ are also plotted. In these models the TP-AGB energetics was calibrated with previous (FMB90, F95) intermediate-age MC cluster data (see Maraston 1998 for full details). Our new observations nicely confirm the modeling and those early results. Old canonical models of stellar evolution (Renzini & Buzzoni 1986) were dating the occurrence of the AGB PT by Renzini & Buzzoni (1986) at significantly earlier epochs (≈10^7 yr) of the stellar lifetime with respect to the new models. This discrepancy is due to a different treatment for the TP-AGB stars that experience the envelope-burning process (Renzini & Voli 1981; Bloecker & Schoenberner 1991), as widely discussed in Maraston (1998).

As further evidence, Figure 8 shows the ratio between the number of C stars and total bolometric luminosity and the ratio between the *K* luminosity of C stars and the total *K*-band cluster luminosity, as a function of the cluster age. The number of C stars in each cluster is listed in Table 3. We assumed that all these stars are cluster members. Indeed, we estimate that the probability of finding a field C star within the sampled cluster area is <30%. The contribution of C stars to the total cluster luminosity as a function of the cluster age closely follows that shown by the entire AGB population (see Fig. 7), and it turns out to be larger than 50% in the 700–1000 Myr age range. In NGC 2190 (with $s = 36$ and hence $t = 730$ Myr) the C stars account for 70% of its total luminosity. Previous work by FMB90 also found that the fraction of luminosity from bright AGB and C stars is maximum for SWB V clusters (i.e., *s* between 35 and 40).

It is worth noting the case of NGC 2249, whose age ($\log t = 8.72$) corresponds to the epoch when the AGB contribution is expected to reach its maximum. Conversely, both Figures 7 and 8 show that NGC 2249 (*open circle*) has a very low AGB luminosity for its age. Indeed, no C stars and only one AGB have been detected in this cluster. On the other hand, NGC 2249 is the least luminous cluster in our sample ($L_K \approx 5 \times 10^4\ L_\odot$); hence, the fastest evolutionary stages (such as the AGB) are expected to be intrinsically poorly populated in its CMD.

7. THE RGB PHASE TRANSITION

For the analysis of the RGB PT we have considered the clusters in our database with $s > 34$ (the six oldest clusters in the sample presented here and the six discussed in F04). Obviously the seven youngest clusters in our sample (Fig. 1) are not considered in the following discussion because they have not developed a populous RGB yet. The considered sample covers a wide range of ages (from 500 Myr to 3.5 Gyr), significantly extending the age range covered by F04, and it allows us to probe the entire development of the RGB.

In order to compute the RGB population ratios we have adopted the same procedure described in F04. Using the cumulative K_0, $(J - K)_0$ CMD for the 12 clusters, we identified the

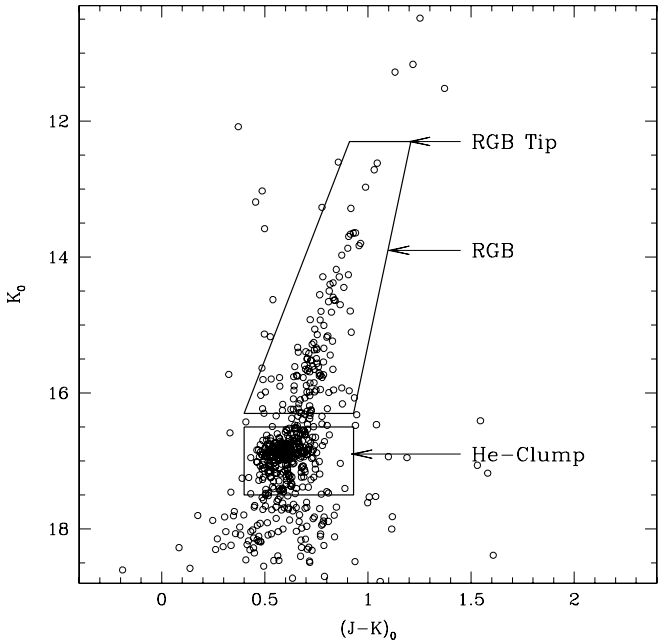

FIG. 9.—An example of a K_0, $(J-K)_0$ dereddened CMD with the selection boxes adopted to distinguish the RGB and the He-clump populations for clusters with $s > 39$ (see Fig. 3). The position of the RGB tip is also indicated.

mean loci of the upper RGB and the He clump and defined the corresponding selection boxes sampling these populations (see F04). As discussed in § 6 the RGB tip is expected to be at $K_0 \approx 12.3$. As an example, Figure 9 shows the dereddened CMD of NGC 1651, where the two selection boxes for the RGB and He-clump population, respectively, have been plotted.

Since the photometric errors can significantly broaden the faint sequences, the size of the boxes including the base of the RGB and the He clump has been conservatively assumed to be ≈5 times the photometric error at that level of magnitude.[4]

Population counts and luminosities for stars in the RGB and He-clump evolutionary stage have been obtained and corrected for incompleteness and field contamination according to the procedure discussed in § 5.1. The results are listed in Table 4 and plotted in Figures 10 and 11. Figure 10 shows the behavior of the number of RGB stars normalized to the number of He-clump stars as a function of the cluster age. Figure 11 shows the bolometric luminosities of RGB stars normalized to the bolometric luminosities of He-clump stars as a function of the cluster age (*top*) and the bolometric luminosities of RGB stars normalized to the bolometric luminosities of entire cluster as a function of age (*bottom*).

Note that in a few high-density clusters (see Table 4) with severe crowding, completeness drops down to 60% at the He-clump magnitude level in the innermost region (see Fig. 5, *region* A). Hence, in these clusters star counts and luminosities have been computed only in the outer regions (*regions* B *and* C).

As already discussed in F04, at an age of ≈500 Myr the rapid increase of the RGB population ratios (by a factor of ≈3 in number and ≈4 in luminosity) in a timescale as short as ≈400 Myr flags the occurrence of the RGB PT. At the age of ≈900 Myr a progressive flattening of the ratios suggests that the full development of an extended and well-populated RGB has occurred.

[4] Note that since the boxes sample the bulk of the population along each evolutionary stage, a slightly different assumption in the selection box size has a negligible impact on the overall results.

TABLE 4

STAR COUNTS AND BOLOMETRIC LUMINOSITIES FOR RGB AND HE-CLUMP STARS

Cluster	s	N_{RGB}[a]	$N_{He\ clump}$[a]	L^{bol}_{RGB} ($10^4\ L_\odot$)	$L^{bol}_{He\ clump}$ ($10^4\ L_\odot$)	Reference
NGC 2249.....	34	9	98	0.16	0.51	F04
NGC 1987.....	35	42	322	0.92	2.05	F04
NGC 2209.....	35	24	160	0.61	0.81	F04
NGC 2108.....	36	40	231	1.11	1.38	F04
NGC 2190.....	36	28	174	0.94	0.89	F04
NGC 2231.....	37	36	114	0.71	0.59	F04
NGC 1783[b].....	37	150	352	4.58	1.98	This paper
NGC 1651.....	39	43	177	1.16	1.09	This paper
NGC 2162.....	39	40	143	0.99	0.78	This paper
NGC 1806[b].....	40	75	218	2.25	1.30	This paper
NGC 2173.....	42	36	84	1.11	0.48	This paper
NGC 1978[b].....	45	182	402	5.03	2.23	This paper

[a] Star counts are corrected for incompleteness and field contamination.
[b] Due to severe crowding conditions, star counts and luminosities have been computed only in the outer B and C regions; see Fig. 5.

The overall increase of the population ratios between ≈500 Myr and ≈3.5 Gyr is a factor of ≈5 by number and ≈7 by luminosity. Empirical data have been compared to theoretical predictions. In Figures 10 and 11, we overplotted the predictions of canonical models (Maraston 1998, 2005) with $[Z/H] = -0.33$. The models nicely agree with the observations over the entire range of considered ages, well describing the epoch, the duration, and the increasing contribution of the RGB phase.

It is worth noting the population ratio excess (both by number and by luminosity; see Figs. 10 and 11) of NGC 1783, when compared with other clusters with similar values of the s-parameter (i.e., NGC 2231). It is likely that this cluster is older than suggested by the s-parameter, since its CMD (see Fig. 3) shows a fully populated RGB, typical of clusters with $s \geq 40$. Indeed,

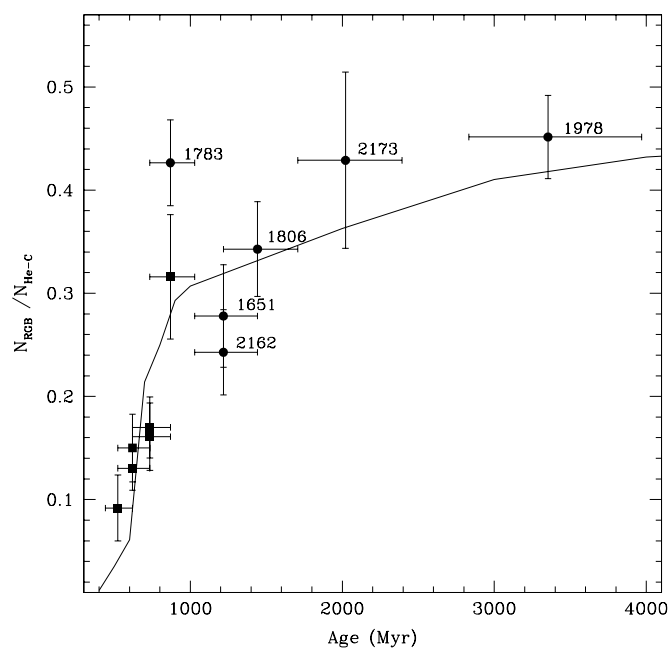

FIG. 10.—Ratio between the number of the bright RGB and He-clump stars as a function of age for the 12 clusters with $s > 33$. The filled circles show the six clusters with $s = 39$–45 presented in this paper (see Fig. 3), and the filled squares show the six clusters from F04. Stars belonging to the two populations are selected according to the selection boxes shown in Fig. 9. The solid line represents the prediction of the canonical theoretical model with $[Z/H] = -0.33$ (Maraston 1998).

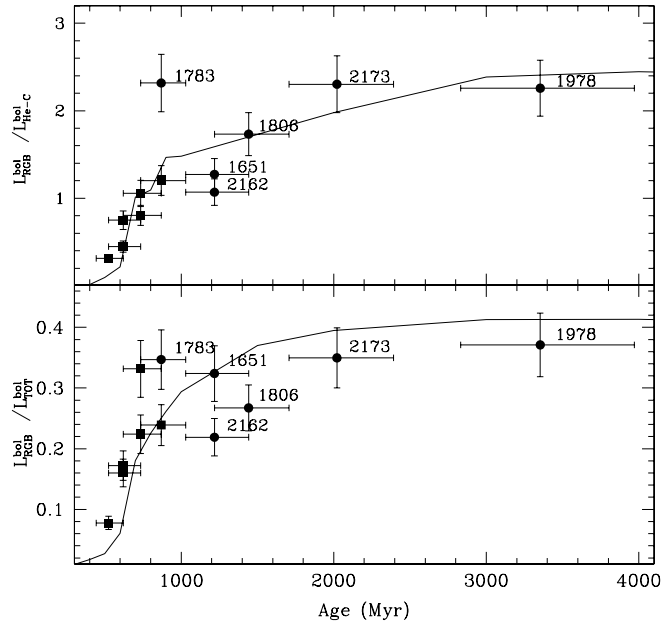

FIG. 11.—*Top*: Bolometric luminosity of the RGB normalized to the He clump as a function of age for the 12 clusters with $s > 33$. Symbols and lines are the same as in Fig. 10. *Bottom*: Bolometric luminosity of the RGB normalized to the total bolometric luminosity for the 12 clusters.

its RGB morphology is more similar to that of clusters such as NGC 1806, NGC 2173, and NGC 1978 rather than that of NGC 2231 (see Fig. 2 in F04). This evidence further supports the urgency of a new homogeneous calibration of the age scale of LMC clusters.

8. CONCLUSIONS

We have used our extensive near-IR database of 19 LMC clusters spanning a wide range of ages (from 80 Myr to 3.5 Gyr) in order to investigate the development in time of the AGB and RGB evolutionary stages.

The behavior of the quantitative contribution to the total cluster luminosity of both the RGB and AGB in terms of age has been investigated and turns out to be nicely in agreement with theoretical predictions of canonical models. The AGB contribution to the total cluster luminosity starts to be significant at ≈200 Myr and reaches its maximum peak at 500–600 Myr (see Fig. 7), when the RGB PT is starting (see F04 and Figs. 10 and 11). Both events are sharp and last a few hundred megayears only.

The epoch and duration of the AGB phase transition estimated from our data confirm the semiempirical modeling of Maraston (1998, 2005). The latter was based on the calibration of the AGB fuel consumption of canonical tracks, and its partition between C- and O-type stars, with previous MC globular cluster data (FMB90, F95). Furthermore, the epoch and duration of the RGB phase transition derived from our data agree very well with the theoretical predictions of simple stellar population models based on canonical tracks and the fuel-consumption approach (Maraston 2005).

This study represents a further step toward the calibration of the integrated properties of SSPs as a powerful diagnostic for dating complex stellar populations such as galaxies.

The financial support by the Ministero dell'Istruzione, Università e Ricerca (MIUR) is kindly acknowledged.

REFERENCES

Alves, D. R. 2004, NewA Rev., 48, 659
Bertelli, G., Bressan, A., Chiosi, C., Fagotto, F., & Nasi, E. 1994, A&AS, 106, 275
Bessell, M. S., & Brett, J. M. 1988, PASP, 100, 1134
Blanco, V. M., Blanco, B. M., & McCarthy, M. F. 1980, ApJ, 242, 938
Bloecker, T., & Schoenberner, D. 1991, A&A, 244, L43
Brocato, E., Di Carlo, E., & Menna, G. 2001, A&A, 374, 523
Bruzual, A. G., & Charlot, S. 1993, ApJ, 405, 538
Calzetti, D., de Marchi, G., Paresce, F., & Shara, M. 1993, ApJ, 402, L1
Cioni, M.-R. L., Girardi, L., Marigo, P., & Habing, H. J. 2006, A&A, 448, 77
Cioni, M.-R. L., & Habing, H. J. 2003, A&A, 402, 133
Dirsch, B., Richtler, T., Gieren, W. P., & Hilker, M. 2000, A&A, 360, 133
Elson, R. A., & Fall, S. M. 1985, ApJ, 299, 211
———. 1988, AJ, 96, 1383
Ferraro, F. R., Fusi Pecci, F., Testa, V., Greggio, L., Corsi, C. E., Buonanno, R., Terndrup, D. M., & Zinnecker, H. 1995, MNRAS, 272, 391 (F95)
Ferraro, F. R., Origlia, L., Testa, V., & Maraston, C. 2004, ApJ, 608, 772 (F04)
Ferraro, F. R., Sills, A., Rood, R. T., Paltrinieri, B., & Buonanno, R. 2003, ApJ, 588, 464
Frogel, J. A., Mould, J. R., & Blanco, V. M. 1990, ApJ, 352, 96 (FMB90)
Frogel, J. A., Persson, S. E., Aaronson, M., & Matthews, K. 1978, ApJ, 220, 75
Girardi, L., Chiosi, C., Bertelli, G., & Bressan, A. 1995, A&A, 298, 87
Hilker, M., Richtler, T., & Stein, D. 1995, A&A, 299, L37
Hill, V., Francois, P., Spite, M., Primas, F., & Spite, F. 2000, A&A, 364, L19
Iben, I., Jr., & Renzini, A. 1983, ARA&A, 21, 271
Maraston, C. 1998, MNRAS, 300, 872
Maraston, C. 2005, MNRAS, 362, 799
Mateo, M. 1988, ApJ, 331, 261
Montegriffo, P., Ferraro, F. R., Fusi Pecci, F., & Origlia, L. 1995, MNRAS, 276, 739
Montegriffo, P., Ferraro, F. R., Origlia, L., & Fusi Pecci, F. 1998, MNRAS, 297, 872
Moorwood, A. F. M., Cuby, G. J., & Lidman, C. 1998, ESO Messenger, 91, 9
Olszewski, E. W., Schommer, R. A., Suntzeff, N. B., & Harris, H. C. 1991, AJ, 101, 515
Persson, S. E., Aaronson, M., Cohen, J. G., Frogel, J. A., & Matthews, K. 1983, ApJ, 266, 105
Persson, S. E., Murphy, D. C., Krzeminski, W., Roth, M., & Rieke, M. 1998, AJ, 116, 2475
Renzini, A., & Buzzoni, A. 1986, in Spectral Evolution of Galaxies, ed. C. Chiosi & A. Renzini (Dordrecht: Reidel), 195
Renzini, A., & Voli, M. 1981, A&A, 94, 175
Rieke, G. H., & Lebofsky, M. J. 1985, ApJ, 288, 618
Sagar, R., & Pandey, A. K. 1989, A&AS, 79, 407
Schlegel, D. J., Finkbeiner, D. P., & Davis, M. 1998, ApJ, 500, 525
Searle, L., Wilkinson, A., & Bagnuolo, W. G. 1980, ApJ, 239, 803 (SWB)
Stetson, P. B. 1987, PASP, 99, 191
Testa, V., Ferraro, F. R., Fusi Pecci, F., Chieffi, A., Straniero, O., & Limongi, M. 1999, AJ, 118, 2839
van den Bergh, S. 1981, A&AS, 46, 79
———. 1998, PASP, 110, 1377